

Portland State University

PDXScholar

Mechanical and Materials Engineering Faculty
Publications and Presentations

Mechanical and Materials Engineering

9-2022

Identifying Population Hollowing Out Regions and Their Dynamic Characteristics across Central China

Bin Guo

University of Science and Technology, Xi'an

Yi Bian

Xi'an University of Science and Technology, Xi'an

Lin Pei

Xi'an Physical Education University, Xi'an

Xiaowei Zhu

Portland State University

Dingming Zhang

Xi'an University of Science and Technology, Xi'an

See next page for additional authors

Follow this and additional works at: https://pdxscholar.library.pdx.edu/mengin_fac



Part of the [Mechanical Engineering Commons](#)

Let us know how access to this document benefits you.

Citation Details

Guo, B., Bian, Y., Pei, L., Zhu, X., Zhang, D., Zhang, W., ... & Chen, Q. (2022). Identifying Population Hollowing Out Regions and Their Dynamic Characteristics across Central China. *Sustainability*, 14(16), 9815.


This Article is brought to you for free and open access. It has been accepted for inclusion in Mechanical and Materials Engineering Faculty Publications and Presentations by an authorized administrator of PDXScholar. Please contact us if we can make this document more accessible: pdxscholar@pdx.edu.

Authors

Bin Guo, Yi Bian, Lin Pei, Xiaowei Zhu, Dingming Zhang, Wencai Zhang, Xianan Guo, and Qiuji Chen

Article

Identifying Population Hollowing Out Regions and Their Dynamic Characteristics across Central China

Bin Guo ^{1,†} , Yi Bian ^{1,†}, Lin Pei ^{2,3,*}, Xiaowei Zhu ^{4,*}, Dingming Zhang ¹, Wencai Zhang ¹, Xianan Guo ¹ and Qiuji Chen ¹

¹ College of Geomatics, Xi'an University of Science and Technology, Xi'an 710054, China

² School of Exercise and Health Sciences, Xi'an Physical Education University, Xi'an 710068, China

³ School of Public Health, Xi'an Jiaotong University, Xi'an 710043, China

⁴ Department of Mechanical and Materials Engineering, Portland State University, Portland, OR 97207, USA

* Correspondence: pl880512@stu.xjtu.edu.cn (L.P.); xz3@pdx.edu (X.Z.)

† These authors contributed equally to this work.

Abstract: Continuous urbanization and industrialization lead to plenty of rural residents migrating to cities for a living, which seriously accelerated the population hollowing issues. This generated series of social issues, including residential estate idle and numerous vigorous laborers migrating from undeveloped rural areas to wealthy cities and towns. Quantitatively determining the population hollowing characteristic is the priority task of realizing rural revitalization. However, the traditional field investigation methods have obvious deficiencies in describing socio-economic phenomena, especially population hollowing, due to weak efficiency and low accuracy. Here, this paper conceives a novel scheme for representing population hollowing levels and exploring the spatiotemporal dynamic of population hollowing. The nighttime light images were introduced to identify the potential hollowing areas by using the nightlight decreasing trend analysis. In addition, the entropy weight approach was adopted to construct an index for evaluating the population hollowing level based on statistical datasets at the political boundary scale. Moreover, we comprehensively incorporated physical and anthropic factors to simulate the population hollowing level via random forest (RF) at a grid-scale, and the validation was conducted to evaluate the simulation results. Some findings were achieved. The population hollowing phenomenon decreasing gradually was mainly distributed in rural areas, especially in the north of the study area. The RF model demonstrated the best accuracy with relatively higher R^2 (Mean = 0.615) compared with the multiple linear regression (MLR) and the geographically weighted regression (GWR). The population hollowing degree of the grid-scale was consistent with the results of the township scale. The population hollowing degree represented an obvious trend that decreased in the north but increased in the south during 2016–2020 and exhibited a significant reduction trend across the entire study area during 2019–2020. The present study supplies a novel perspective for detecting population hollowing and provides scientific support and a first-hand dataset for rural revitalization.

Keywords: population distribution; random forest; nighttime light; modeling; remote sensing



Citation: Guo, B.; Bian, Y.; Pei, L.; Zhu, X.; Zhang, D.; Zhang, W.; Guo, X.; Chen, Q. Identifying Population Hollowing Out Regions and Their Dynamic Characteristics across Central China. *Sustainability* **2022**, *14*, 9815. <https://doi.org/10.3390/su14169815>

Academic Editor: Antonio Miguel Martínez-Graña

Received: 6 June 2022

Accepted: 5 August 2022

Published: 9 August 2022

Publisher's Note: MDPI stays neutral with regard to jurisdictional claims in published maps and institutional affiliations.



Copyright: © 2022 by the authors. Licensee MDPI, Basel, Switzerland. This article is an open access article distributed under the terms and conditions of the Creative Commons Attribution (CC BY) license (<https://creativecommons.org/licenses/by/4.0/>).

1. Introduction

Three rural issues, including agriculture, countryside, and farmers, have been arousing wide concerns by scholars and have been becoming a top priority of the mission of the central government of China recently [1]. The rural revitalization strategy released by the 19th National Congress of the Communist Party of China in 2017 has set a goal to address the three rural issues, especially the disbalance in terms of urban agglomerations and rural regions development as well as deficient rural development [2]. The priority obstacle among the three rural issues is the rural population hollowing out [3]. Population hollowing out mainly leads to two serious issues. On the one hand, the rural residents,

especially large numbers of young and vigorous laborers, flock to cities for a living; on the other hand, the rural land resources have been continuously occupied without reasonable planning, but the old residential estate has not been demolished, which led to the phenomenon of “external sprawl, internal chaos” [4]. What is more, the rural demographic structure, especially the quality of the population, has been severely affected by population hollowing out. The rural demographic structure exhibits senior and children accumulation, but adults lose features accompanying a variety of social issues such as land idle and poverty acceleration [5]. The main reason for the population hollowing out is the accelerated urbanization and the continuous urban–rural transformation process [6]. China, the largest developing country in the world, has to fill the gap of the imbalance in development in urban and rural areas and server environmental issues, especially air pollution [7]. Although the speed of urbanization in China is significant, the aggrandizement of population hollowing out featured by the decreasing of the population in rural regions, numerous abandoned and idle estates were generated due to massive population migration between urban and rural areas in the past decades [8,9]. The main aims of the Central Committee No.1 document disclosed in 2018 were realizing rural revitalization and solving the rural hollowing issue [10]. Hence, it is urgent to solve the population hollowing out issues for further realizing rural revitalization [11].

One of the key processes for describing the population hollowing out is that quantitatively determine the accurate population distribution timely [12]. In contrast, the previous population data with the administrative boundary are coarse for the updating frequency and not enough [13]. Meanwhile, the spatial heterogeneity of population distribution within the political division was always neglected, for the accuracy of the traditional dataset is limited [14]. Furthermore, the previous survey approaches were time and finance-consuming [15]. Therefore, it is indispensable to develop a reasonable method to calibrate the population distribution on the grid-scale to improve the accuracy of the dataset. Fortunately, remote sensing technology supplies a possibility for retrieving social–economic parameters [16]. Previous studies have attempted to infer social–economic conditions using large data, including remotely sensed data and social media data. Large data such as social media data, the points of interest (POIs) [17,18], street view pictures [19], mobile phone metadata [20], public transit smartcard data [21], and housing rent data [22] as well as the remotely sensed data have been widely used to predict socio-economic parameters such as population [23–26], electricity consumption [27,28], the built-up area detection [29,30], gross domestic product [31], poverty [32], house vacancy [33], and can be better used in the fields of describing the socio-economic conditions of urban interior space. Although the spatiotemporal resolution has been greatly improved and the cost of data acquisition has been largely reduced by the big data, using big data to determine the population hollowing out was still a big challenge. To our knowledge, the population hollowing out issues are not only affected by natural factors but also influenced by anthropic factors. Published studies mainly evaluated socio-economic phenomena from a single perspective. However, identifying the population hollowing out issues are more complicated than a single socio-economic phenomenon, and the concept of population hollowing out needs to be comprehensively described using multi-source data based on multiple perspectives. Additionally, previous studies on population hollowing out were mainly concentrated on its connotation and formation mechanism [34], evolution law and stage features [35], affecting factors and driving forces [36,37], reclamation potential and measure [38], policy-making, et al. [39–42]. Overall, most published research focused on the quantitative determination and regional spatial heterogeneity of population hollowing out at political boundary scale on a single time cross-section. However, the spatial and temporal dynamics of population hollowing out issues at the grid-scale were seldom reported.

Shanxi, Hubei, Hunan, Anhui, Henan, and Jiangxi, located in central China, are some of the important food production bases, energy raw material bases, equipment manufacturing bases, and Chinese comprehensive transportation hub [43]. In past decades, a large number of rural estate was idle and improvident because numerous rural people

migrated into urban areas in central China. The inadequate resources, dense population, undeveloped infrastructure, and complicated physical geography and topographic conditions may lead to population loss. The population hollowing out issues of the six central provinces in China was not only a simple phenomenon that the rural laborers move from the countryside to cities and towns but also a serious social issue that a larger number of young human resources transferred from underdeveloped rural regions to developed urban regions [44]. Consequently, the population hollowing out issues of the six central provinces in China are more typical, and conducting related studies is strongly desired currently. So, the significant contribution of this study is to propose a novel scheme for quantitatively estimating the population hollowing out level via multiple models based on nighttime light remotely sensed images and other auxiliary spatial–temporal data in six provinces of Central China.

Based on the above, the objectives of this study are: (i) to take six provinces of Central China as the research object, construct a population hollowing index, and calibrate the population hollowness level at grid and township scale based on RF, geographically weighted regression (GWR), and multiple linear regression using Multi-source spatiotemporal big data during 2016–2020, (ii) to validate the calibration results based on actual statistical data, and (iii) to analyze the spatial pattern of the population hollowing out and explore its spatial–temporal dynamic characteristics.

2. Study Area and Materials

2.1. Study Area

The six central provinces of China, with about 1.03 million km², have diverse landscapes, including mountains, rivers, and plains. The six central provinces with great rainfall conditions are located in a monsoon climate zone. The areas of the urban region and rural region in the six central provinces are 1.15 and 3.18 ten thousand km², respectively [45]. The population and the gross domestic product (GDP) of the six central provinces account for 28.1% of the Chinese population and 20% of the entire GDP of China [46]. The location and landcover map of the study area are shown in Figure 1.

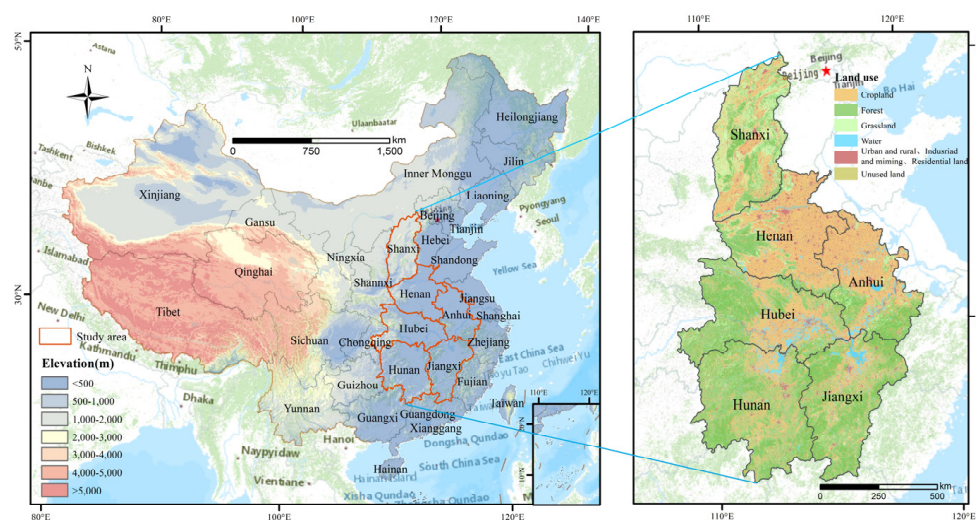


Figure 1. The location and landcover map of the study area. **Note:** The six central provinces' land use (the year 2020) data are made available by the data center of resources and environmental sciences, Chinese Academy of Sciences <http://www.resd.cn> (accessed on 1 January 2021).

2.2. Data Sources and Pretreatment

The data used in the present study, including the physical and human geography dataset, are listed in Table 1. Specifically, the physical geography dataset consisted of digital elevation model (DEM) data, water vector data, meteorological factors, and normalized difference vegetation index (NDVI) data.

Table 1. Description of the datasets.

Sorts	Factors	Sources	Resolution
Physical geography	DEM	http://www.gscloud.cn/ (accessed on 1 January 2021).	2015 (30 m)
	Waterbody density (WD)	http://www.openstreetmap.org/ (accessed on 1 January 2021).	2016–2020 (Vector data)
	Meteorological factors concerning Atmospheric pressure (PRS), Relative humidity (RHU), Temperature (TEM), Wind speed (WIN), Precipitation (PRE)	http://data.cma.cn/ (accessed on 1 January 2021).	2016–2020 (Monthly ground-level monitoring station data)
	NDVI	https://modis.gsfc.nasa.gov/ (accessed on 1 January 2021).	2016–2020 (250 m)
Human geography	Point of interest (POI)	http://www.openstreetmap.org/ (accessed on 1 January 2021).	2016–2020 (Vector data)
	Road density (RD)		
	GDP	Statistical yearbook, The statistical report, the official website of each regional statistical bureau, Census report	2016–2020 (township)
	Population Statistical data		
	Related agricultural data		
	Population density (POP)	https://www.worldpop.org/ (accessed on 1 January 2021).	2016–2020 (1000 m)
	NPP-VIIRS Monthly nighttime stable light (NTL) composite data	https://ngdc.noaa.gov/ (accessed on 1 January 2021).	2016–2020 (742 m)
	Global NPP-VIIRS-like nighttime light data	http://doi.org/10.7910/DVN/YGIVCD (accessed on 1 January 2021).	2000–2015 (15 arc seconds)
	Air Pollutants (CO, NO ₂ , O ₃ , PM ₁₀ , PM _{2.5} , SO ₂)	http://www.cnemc.cn/ (accessed on 1 January 2021).	2016–2020 (Hourly ground-level monitoring station data)

The human geography dataset includes POI data, road vector data, GDP data, population data, nighttime stable light data, air pollutants data, and related agricultural data. The POI data and road vector data were collected from the wiki world map database <http://www.openstreetmap.org/> (accessed on 1 January 2021). The GDP data, population statistical data, and related agricultural data were made available from the statistical yearbook, statistical report, and official website of the local statistical bureau. The population statistical data include the registered population, the permanent population, the total population, the rural permanent population, the total rural population, and the rural employees. Population (POP) raster data were obtained from the world pop website <https://www.worldpop.org/> (accessed on 1 January 2021), and the total number of people classified by gender and age sets (including 0–14 and over 65) for each grid was calculated in the study area during 2016–2020. Nightlight images were downloaded from <https://ngdc.noaa.gov/> (accessed on 1 January 2021), and global NPP-VIIRS-like nighttime light data were obtained from <http://doi.org/10.7910/DVN/YGIVCD> (accessed on 1 January 2021) during 2000–2015 [47]. In addition, the hourly-averaged air observations during 2016–2020 were from China Environment Monitoring Center (CNEMC).

The data preprocessing is stated below. The raw NPP-VIIRS (Suomi National Polar-orbiting Partnership-Visible Infrared Imaging Radiometer Suite) NTL (nighttime light) data have deviation due to the impact of clouds, moonlights, stray lights, fires, volcanoes, gas flares, background noise, and other ephemeral lights. The raw NPP-VIIRS NTL data have been processed to remove outliers in the present study. Moreover, annual NPP-VIIRS NTL data were synthesized from correspondence monthly NPP-VIIRS nighttime light data. All images were resampled to a spatial resolution of 500 m. China Geodetic Coordinate System

(CGCS2000) was selected as a coordinate reference for all datasets, and all layers were reclassified into 500 m resolution via ArcGIS 10.0 to keep consistency [48]. We processed missing data and outliers before constructing the database [49]. We used MATLAB, Excel, ArcGIS10.0, R, and ENVI for data pretreatment, analysis, and mapping. The ordinary Kriging interpolation method was used to interpolate data into 500 m grid layers [50]. The zonal statistics tool, tabulate intersection, and summary statistics of ArcGIS10.0 were used to construct the database [51].

Unit: CO (mg/m^3), NO₂, O₃, PM₁₀, PM_{2.5} and SO₂ ($\mu\text{g}/\text{m}^3$); PRS (hPa), RHU (%), TEM ($^{\circ}\text{C}$), WIN (m/s), PRE (mm); DEM (m), WD, and RD (m/m^2), POP (person/ hm^2), NTL ($\text{W}/\text{cm}^2/\text{sr}$), GDP (RMB 100 million), NDVI (unitless). Note: population statistical data and related agricultural data were used to calculate PHI at a township scale via Equation (1) and Table 2, and other data listed in Table 1 were adopted to fit RF and MLR models and to map PHI distributions at a grid-scale.

Table 2. PHI and weights for each indicator.

Indicators	Weights	Effects	Calculation Methods
Population outflow rate	0.21	positive	(Registered population–permanent population)/Registered population
The ratio of 0–14 years old to the total population	0.18	positive	0–14 years population/Total population
The ratio of the over 65 population to the total population	0.18	positive	Population over 65/Total population
The ratio of rural permanent population to the total rural population	0.17	negative	Rural permanent population/Total rural population
The ratio of the rural employed population to the total rural population	0.15	negative	Rural employees/Total rural population
Average agricultural land	0.11	positive	Total agricultural land area/Total rural population

3. Methods

3.1. Workflow

The workflow of this research includes three steps that are data collection and preprocessing, model fitting and validation, and the distribution and spatiotemporal dynamic of population hollowing (Figure 2). First, dependent variables and independent variables were collected and processed for further analysis. PHI for each township, calculated in Section 3.2, was selected as dependent variables for Equations (2) and (3). Independent variables' value for each township was obtained via the zonal statistics tool in ArcGIS10.0, and independent variables were listed in Table 1. Second, GWR, regression model, and RF were fitted based on independent variables listed in Table 1 and dependent variable calculated in Section 3.2 to determine the quantitative relation between the dependent variable and independent variables at the township scale [52]. Then the modeling outcomes were validated. Additionally, potential hollow areas in the study area were identified using the decreasing trend detection of the night light images. Third, the optimum model was adopted to map a grid-scale population hollowing distribution. The spatiotemporal dynamic characteristics of population hollowing were obtained.

3.2. Calculation of Population Hollowing Index Based on Statistical Data

$$\text{PHI} = \sum_{j=1}^m W \times P \quad (1)$$

where PHI is the PHI value for each township, m denotes the number of indicator, W is the weight of each indicator of the population hollowing index [53,54], and P is the normalized value of each indicator calculated based on methods from Table 2.

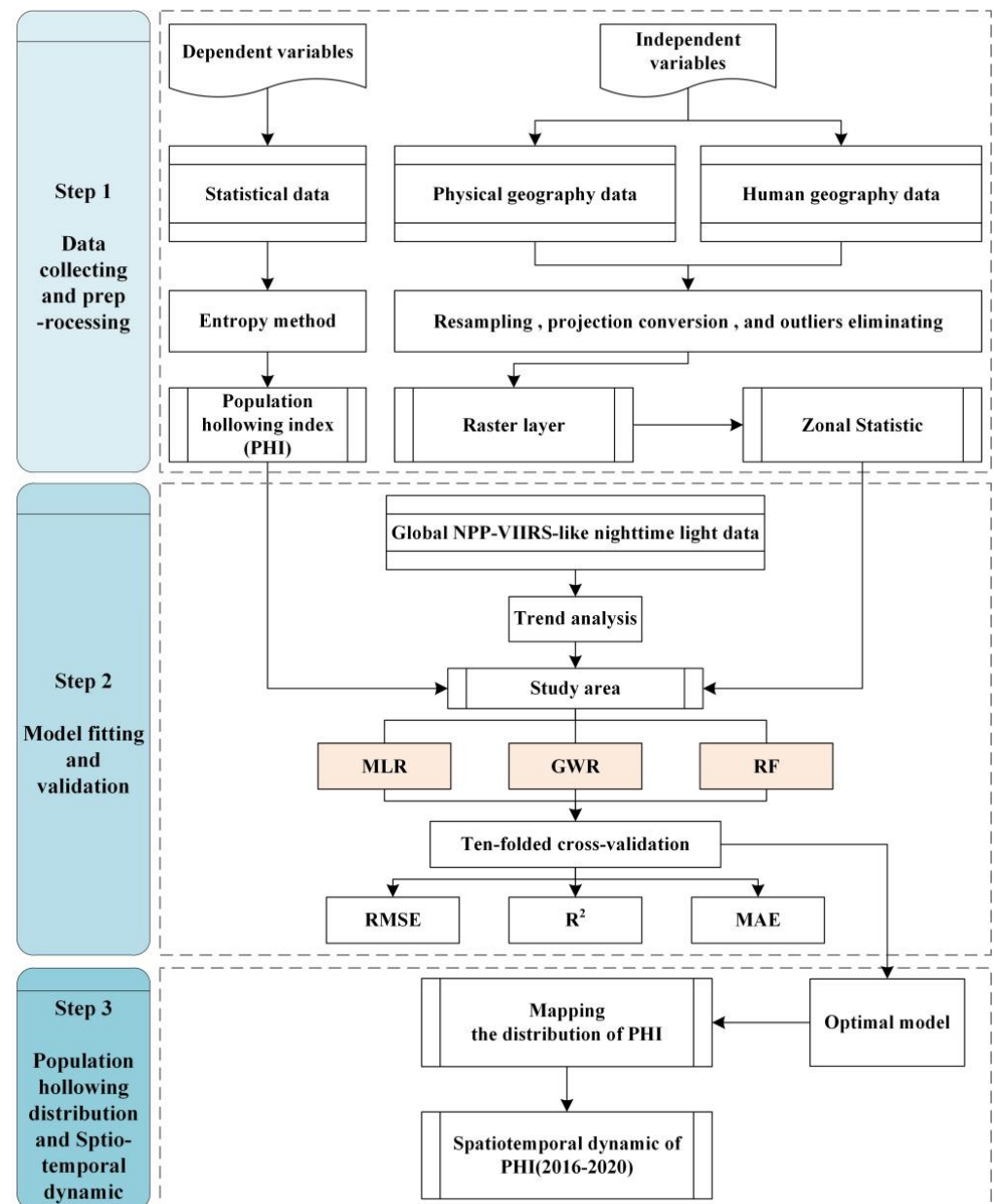


Figure 2. Workflow of the present study.

The indicator values were calculated with the listed methods in Table 2 using the datasets in Table 1, and each indicator value was normalized. The entropy weight method is used to determine the weights for the indicators of the PHI at the township scale in the six provinces of central China. The weights of population outflow rate, the ratio of 0–14 years old to the total population, the ratio of over 65 population to the total population, the ratio of rural permanent population to the total rural population, the ratio of rural employed population to the total rural population, and average agricultural land are 0.21, 0.18, 0.18, 0.17, 0.15, and 0.11, respectively. Additionally, the positive and negative effects of each indicator were determined according to the published reference [55]. The distribution map of the PHI at the township scale of the study area was obtained based on Equation (1), population statistical data, and related agricultural data in Tables 1 and 2 using field calculation in ArcGIS 10.0.

3.3. Fitting PHI Prediction Models on a Political Boundary Scale

3.3.1. Geographically Weighted Regression (GWR)

$$PHI_i = \beta_{0(u_i, v_i)} + \beta_{1(u_i, v_i)} \cdot B_1 + \beta_{2(u_i, v_i)} \cdot B_2 + \dots + \varepsilon_i \quad (2)$$

where β_0 denotes the intercept of a specific position (u_i, v_i) ; the position (u_i, v_i) represents the geometric center coordinates of township i ; β_1 represents the slopes for the factors listed in Table 1 at a specific location (u_i, v_i) ; B_i is the factors' value listed in Table 1; ε_i is the bias of the township i [56–59].

3.3.2. Regression Model

The regression model was used to estimate socio-economic parameters based on remotely sensed data previously [60,61]. The present study selected the regression model as the comparison model for evaluating the performance of simulated results.

$$PHI_i = \gamma_0 + \gamma_1 X_1 + \gamma_2 X_2 + \dots + \varepsilon_a \quad (3)$$

where γ_0 represents the intercept; γ is the slope for each factor listed in Table 1. X denotes the factor's value listed in Table 1; ε_a is the error term for a specific township.

3.3.3. Random Forest (RF)

The RF algorithm, based on regression tree (CART) analysis and classification, is a bagging method [62]. The variable selection number (mtry) when branching, the number of trees of the classification tree (ntree), and the size of the leaf (node size) were necessary for fitting the RF model [63,64]. The detailed information of the RF model can be found in the published paper [65].

3.3.4. Validation

The accuracy was evaluated via the 10-folded cross-validation [66]. The entire samples were reclassified into 10 sets with the same number. Nine sets were selected for fitting models, and the tenth set was utilized for validation. Next, the same process was conducted nine times until 10 sets were chosen once as the validation set. In this work, we introduced determinate coefficients (R^2), root mean square error (RMSE), and the mean absolute error (MAE) to assess accuracy [67–69].

$$R^2 = \frac{\sum_{i=1}^n (PHI_{e,i} - \overline{PHI})^2}{\sum_{i=1}^n (PHI_{t,i} - \overline{PHI})^2} \quad (4)$$

$$MAE = \frac{1}{n} \sum_{i=1}^n |PHI_{t,i} - PHI_{e,i}| \quad (5)$$

$$RMSE = \sqrt{\frac{1}{n} \sum_{i=1}^n (PHI_{t,i} - PHI_{e,i})^2} \quad (6)$$

where n represents the number of township, $PHI_{e,i}$ is the predicted PHI of the township i , PHI is the population hollowing Index, $PHI_{t,i}$ represents the actual PHI of township i , and \overline{PHI} is the actual average PHI of townships.

3.4. Detecting the Distribution and the Dynamic of Population Hollowing

3.4.1. Mapping the PHI on a Grid-Scale

The optimum method with the best accuracy was chosen to illustrate the PHI map. The estimated values of the PHI may have some biases. Therefore, we used an index to correct biases.

$$PHI'_{i,j} = PHI_{i,j} \times \left(\frac{PHI_{i,static}}{PHI_{i,predicted}} \right) \quad (7)$$

where $PHI'_{i,j}$ denotes the corrected PHI grid value at pixel j within township i , $PHI_{i,j}$ denotes the PHI grid value estimated by Equation (2) at pixel j within township i , $PHI_{i, statistic}$ denotes the PHI calculated by Equation (1) using statistical data in Table 2 at township i , $PHI_{j, predicted}$ represents the total PHI grid value at township i , and the total PHI grid value at township i was calculated by zonal statistic tool of ArcGIS 10.0 [70–73].

3.4.2. Detecting the Dynamic of PHI

A trend analysis was used to determine the potential population hollowing areas and map the dynamic of PHI [74]. The tendency of NTL and PHI values variation could be determined using Equations (8) and (9).

$$\text{slope}_1 = \frac{n * \sum_{i=1}^n i * NTL_i - (\sum_{i=1}^n i)(\sum_{i=1}^n NTL_i)}{n * \sum_{i=1}^n i^2 - (\sum_{i=1}^n i)^2} \quad (8)$$

$$\text{slope}_2 = \frac{n * \sum_{i=1}^n i * PHI_i - (\sum_{i=1}^n i)(\sum_{i=1}^n PHI_i)}{n * \sum_{i=1}^n i^2 - (\sum_{i=1}^n i)^2} \quad (9)$$

where NTL_i denotes the DN value of nighttime light images at grid i , PHI_i denotes the PHI value at grid i , and n represents the period; in this paper, $n = 5$, and i is the time unit [75,76]. The potential population hollowing areas were identified based on slope_1 . On the one hand, if the $\text{slope}_1 \leq 0$, it means the total night light of the specific area was decreased, so these regions were considered as one of the potential population hollowing areas. On the other hand, if the $\text{slope}_1 > 0$ at $p \leq 0.05$, significance indicated the total night light of these regions was increased. So, the areas with increasing total night light were excluded from the potential population hollowing areas. The areas with $\text{slope}_1 > 0$ ($p > 0.05$) remained as the other potential population hollowing areas to avoid mistakenly excluding potential population hollowing areas.

The population hollowing trends were identified based on slope_2 . The level of PHI trends was determined by the natural break method in ARCGIS 10.0. The map of PHI was divided into five sorts, including fast reduction, slow reduction, slow growth, moderate growth, and fast growth, according to slope_2 .

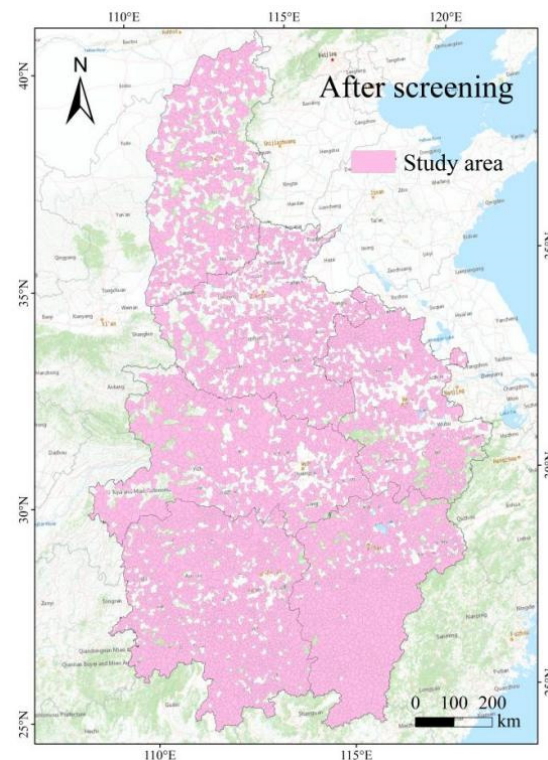
4. Results

4.1. Identifying the Potential Population Hollowing Regions via Trend Analysis Based on NPP-VIIRS-like Nighttime Lights Images

The study area consists of 9254 townships. slope_1 (Equation (8)) was used to determine the potential population of hollowing townships. The number of townships with $\text{slope}_1 > 0$ was 4864. The number of townships with $\text{slope}_1 > 0$ and $p \leq 0.05$ was 2512, revealing that the total night light in these areas was significantly promoted. So, areas with $\text{slope}_1 > 0$ and $p \leq 0.05$ were excluded for the population may be obviously increased in those regions. The number of townships with $\text{slope}_1 \leq 0$ was 4390 that indicating the population may be decreased in those regions because the total night light in these areas was decreased. Hence, the regions with $\text{slope}_1 \leq 0$ were considered as one of the potential population hollowing areas. Finally, the number of potential population hollowing townships was determined after screening according to the rules in Section 3.4 (Table 3). The excluded townships mainly were the areas with subdistrict offices where the rate of urbanization was higher than other regions in the rural areas. Among these excluded townships, parts of them were newly established districts during 2016–2020, such as Taikoo District, Jinzhong City, and Shanxi Province. Obviously, the excluded areas were mainly distributed in the southern and northern parts of the research area, and the number of the excluded areas in the north was larger than in the south. Meanwhile, the distribution features of excluded areas located in Shanxi, Henan, and Anhui were relatively even. The population hollowing areas demonstrated accumulated characteristics in the eastern part of Hubei Province and the northern part of Hunan Province (Figure 3).

Table 3. The number of potential population hollowing townships.

The Total Number of Townships	The Number of Townships with $Slope_1 > 0$	The Number of Townships $Slope_1 > 0$ and $p \leq 0.05$	The Number of Townships with $Slope_1 \leq 0$	The Number of Potential Population Hollowing Townships
9254	4864	2512	4390	6742

**Figure 3.** The study area was determined by using nighttime light remote sensing techniques to retrieve potential population hollowing regions.

4.2. The Evaluation and Comparison of Calibration Models for Population Hollowing

The RF method indicated the best performance with the highest R^2 , lowest RMSE, and MAE among the calibration models, followed by GWR and MLR during 2016–2020. The best outcome was detected in the year 2019, and the RF method demonstrated the best performance with the highest $R^2 = 0.6061$, lowest RMSE = 0.0477, and MAE = 0.0403 among the calibration models, followed by GWR and MLR (Table 4 and Figure 4). Therefore, the RF model was selected for grid-scale population hollowing mapping. In the present work, the optimal prediction outcome was obtained when $mtry = 4$ and $ntree = 500$ were chosen for fitting the RF model.

4.3. The Distribution and Spatiotemporal Dynamic Characteristic of Population Hollowing

It can be seen from Figure 5 that the PHI was serious in the north of the study area but not significant in the south of the study area. Specifically, the severe and moderate PHI are mainly distributed in most of Shanxi Province, the central, eastern, and northeastern parts of Henan Province, the northern part of Anhui Province, most of Hunan Province, and the northern part of Jiangxi Province (Figure 5 with orange and red). One of the severe PHI was detected in the Fenwei Plain located in Shanxi Province, and the other severe PHI was distributed around the provincial capital or areas with better economic development. The most PHI of the other five provinces was mainly accumulated in the central part except for Shanxi Province, but the PHI was slight in remote areas of the five provinces (Figure 5

with yellow and green). Moreover, the population hollowing phenomenon decreased in the study area from 2016 to 2020. It was obvious that the PHI with the highest level in 2016 and with the lowest level in 2020. The most serious PHI with a severe level in 2020 was mainly distributed in Yueyang City (Hunan Province), Shangrao City, and Jiujiang City (Jiangxi Province) (Figure 5).

Table 4. Evaluating calibration models for population hollowing using R^2 , RMSE, and MAE.

2016			2017		2018		2019		2020	
RF	C	V	C	V	C	V	C	V	C	V
R ²	0.6076	0.5882	0.6125	0.6033	0.6087	0.5898	0.6246	0.6061	0.6235	0.5877
RMSE	0.0301	0.0462	0.0216	0.0351	0.0214	0.0311	0.0297	0.0477	0.0295	0.0501
MAE	0.0248	0.0371	0.0167	0.0302	0.0116	0.0251	0.0245	0.0403	0.0244	0.0461
GWR	C	V	C	V	C	V	C	V	C	V
R ²	0.4291	0.3769	0.4425	0.3986	0.4064	0.3751	0.4343	0.4012	0.4289	0.3784
RMSE	0.0763	0.0801	0.0772	0.0869	0.0796	0.0907	0.0737	0.0799	0.0759	0.0844
MAE	0.0681	0.0749	0.0657	0.0705	0.0699	0.0762	0.0676	0.0708	0.0687	0.0738
MLR	C	V	C	V	C	V	C	V	C	V
R ²	0.1022	0.0917	0.1276	0.0619	0.0954	0.0776	0.0879	0.0691	0.1075	0.0641
RMSE	0.0997	0.1864	0.0912	0.1859	0.1033	1.1793	0.1268	0.1854	0.0955	0.1845
MAE	0.0779	0.1254	0.0736	0.1304	0.0802	0.1289	0.0839	0.1201	0.0725	0.1293

Note: C and V denote the calibration and validation for the models, respectively.

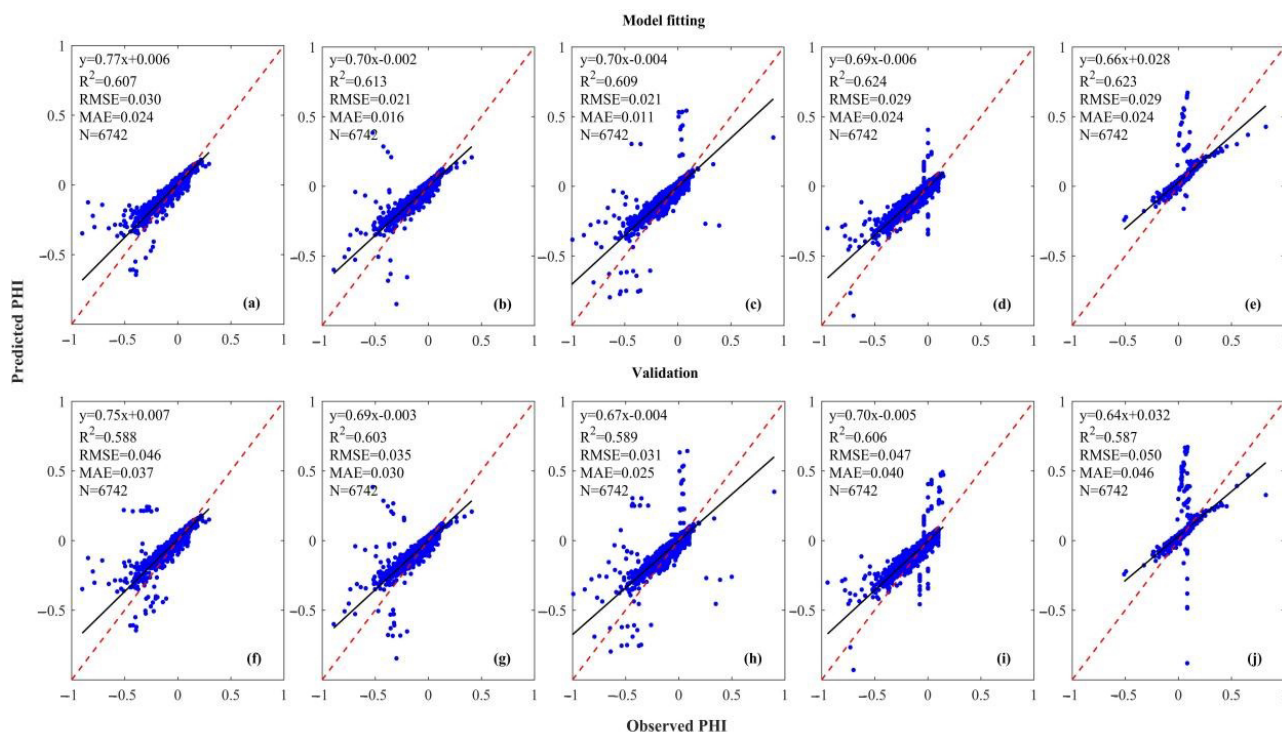


Figure 4. Scatter plots of population hollowing modeling based on RF method during 2016–2020. **Note:** (a) and (f), (b) and (g), (c) and (h), (d) and (i), and (e) and (j), represent 2016, 2017, 2018, 2019, and 2020, respectively.

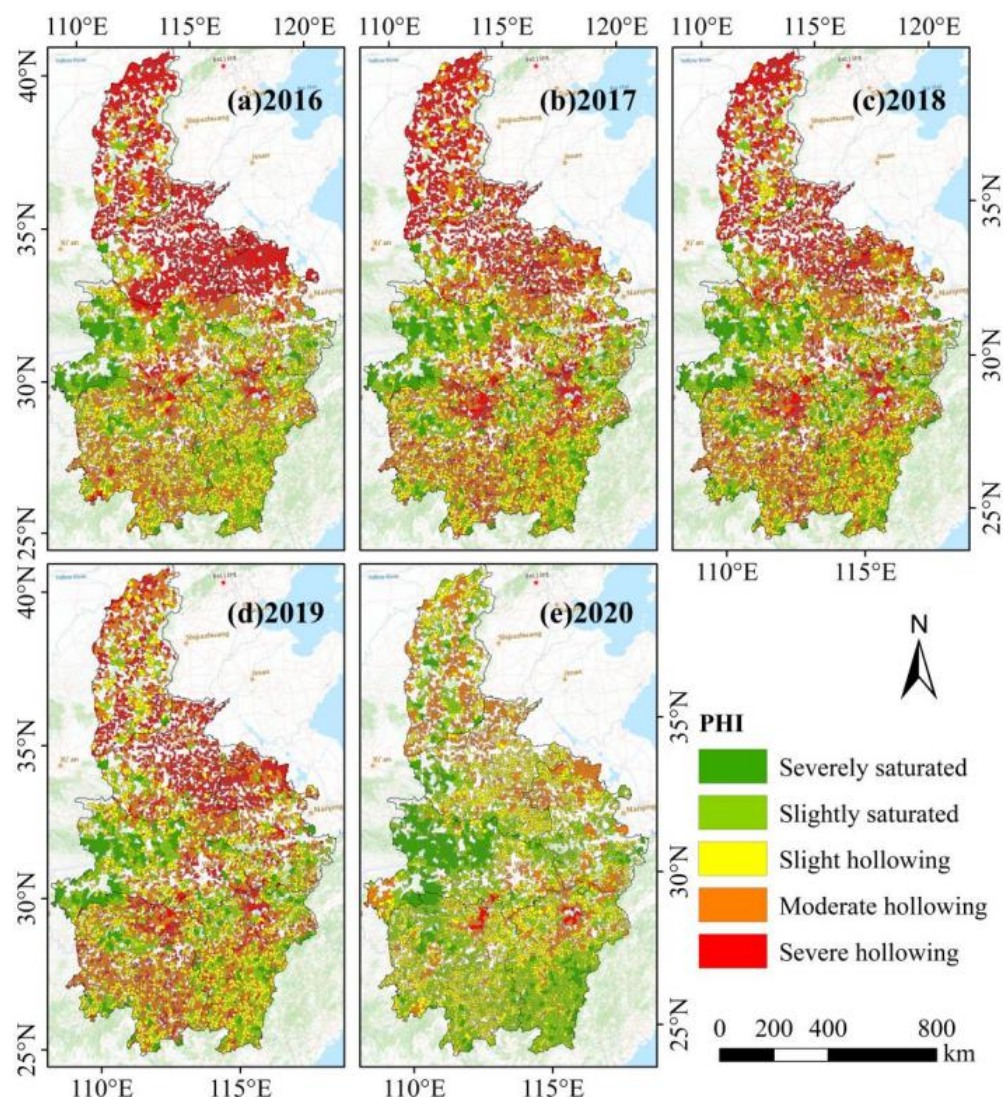


Figure 5. The distribution map of PHI was calculated via Equation (1) at the township scale in six provinces of central China from 2016 to 2020.

The grid-scale distribution of PHI was mapped via the RF method determined by Section 4.3 (Figure 6). Clearly, the distribution of PHI at the grid scale was relatively consistent with the results at the township scale (Figure 5) during 2016–2020 and revealed a similar trend that the PHI was high in the north and low in the south. Furthermore, the detailed information at the grid-scale can be detected via Figure 6 that the uneven distribution features of PHI inside a political boundary can be differentiated. Specifically, the PHI level was more serious at the grid-scale than the township scale in the Fenwei Plain and the Yangzi River watershed areas in the year 2020.

Meanwhile, the spatiotemporal dynamic of PHI at grid-scale in six provinces of central China from 2016 to 2020 was described via trend analysis. Overall, the PHI level demonstrated a decreased trend in the north and a raised trend in the south in the study area from 2016 to 2020. Specifically, most parts of Shanxi Province, eastern and central Henan Province, and northeastern and northern Anhui Province revealed a decreased trend, especially Henan Province.

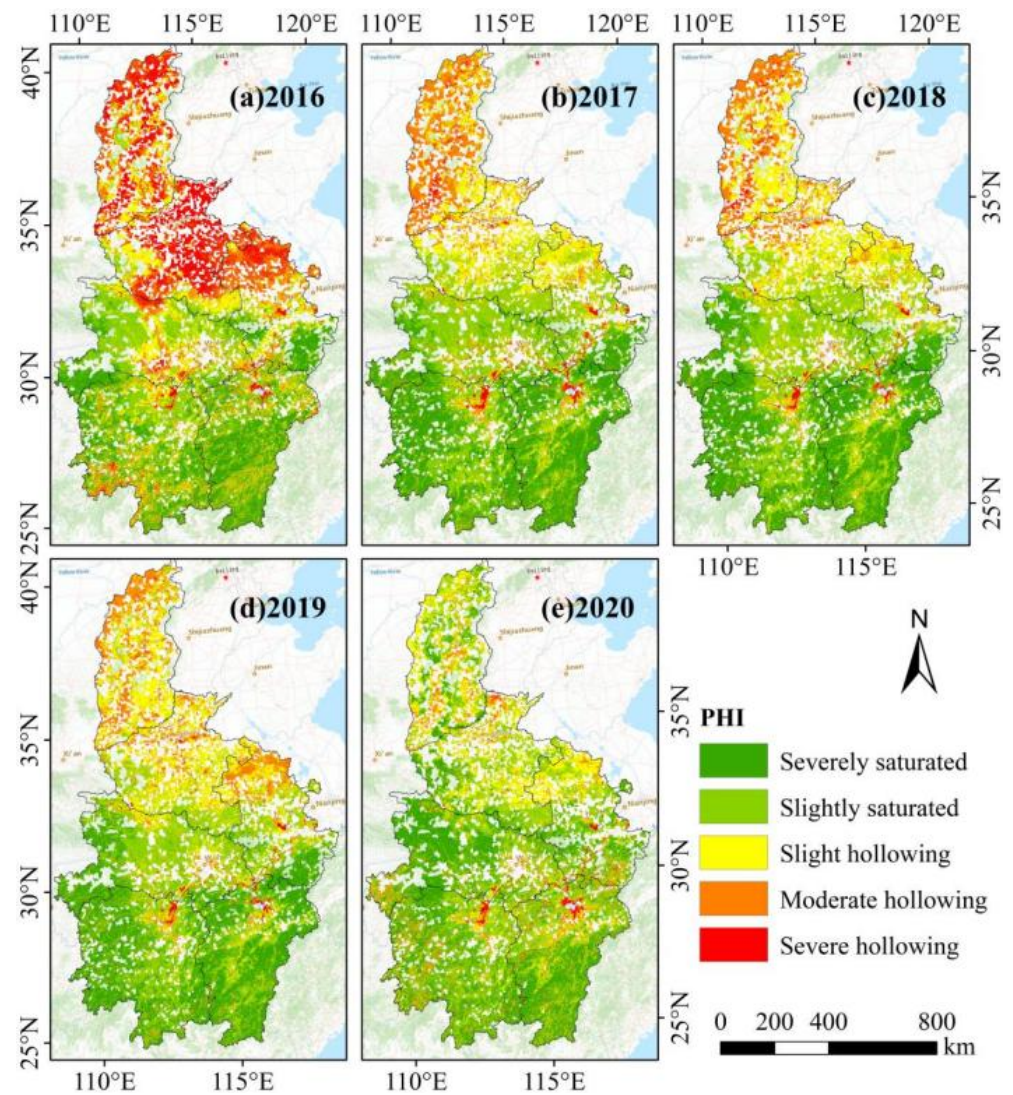


Figure 6. The distribution map of PHI was calibrated via the RF method at a grid-scale in six provinces of central China from 2016 to 2020.

The PHI in the southern part of the study area indicated the fastest upward trend, including areas located in the southwestern of Hubei Province and the northwestern of Hunan Province, the northern of Jiangxi Province as well as the southern of Anhui Province (Figure 7a). Clearly, the building area increased in northern of the study area, including Shanxi, Henan, and Anhui, which was inverse to the PHI decreasing change trend (Figure 7b). That is, the PHI was decreasing in the north of the study area, and which building area was increasing in the correspondence area. The relationship between PHI and building area indirectly proved our simulated PHI outcomes were reliable.

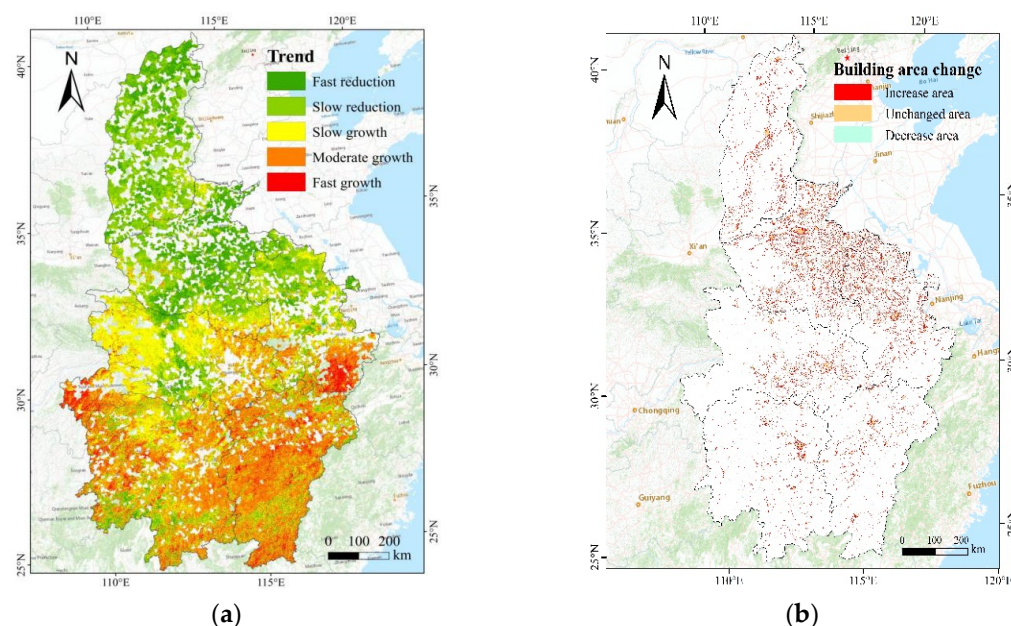


Figure 7. The spatiotemporal dynamic map of PHI (a), and building area (b) at grid-scale in six provinces of central China from 2016 to 2020.

5. Discussion

5.1. The Comparison between Our Scheme and the Previous Studies

The random forest model was adopted as the optimum method for identifying PHI at the grid-scale in this study. The good performance of RF with relatively higher accuracy in estimating socio-economic parameters than traditional methods, including MLR and GWR, has been reported by previous studies [77]. The robustness of RF has also been confirmed by the current study that the accuracy of RF in identifying PHI outperformed other methods, including GWR and MLR. We first extended the published studies that the RF method can be successfully used to identify the population hollowing at a grid-scale. The possible reason for the higher accuracy of the RF method in detecting PHI than any other method was the nonlinear relations between affecting factors and PHI. For example, the PHI was correlated with the location of the natural and human influential factors that have to be considered from a nonlinear perspective. Hence, the accuracy of MLR and GWR was lower than the RF method due to the linear hypothesis [78].

Although previous studies have introduced field surveys to determine PHI [36,37], the field investigation method was time-consuming and expensive and was hard to implement in a larger region. Meanwhile, some scholars used related indicators to infer the PHI level at the political boundary scale. However, the indicators method neglected the subtle details inside the political boundary, and the differences in PHI cannot be detected accordingly. Moreover, field investigations have been seldomly conducted to verify the reliability and feasibility of the indicators method, and the accuracy of the estimation of PHI was doubtful. We improved the accuracy of the PHI estimation model by RF at grid-scale and strengthened the validation process. The outcomes of the present study confirmed that the scheme of this paper could be effectively used to identify PHI in a relatively larger region.

5.2. The Possible Reasons and Explanations for the Distribution and Dynamics of Population Hollowing across the Study Area during 2016–2020

To our knowledge, population hollowing was mainly affected by physical geographical factors, social and economic development, and disasters or unexpected events [79]. Firstly, from the location perspective, the six provinces of central China are adjacent to regions with relatively better economic status, such as Chongqing, and the eastern and southern coastal areas [80]. Our outcomes demonstrated that the population hollowing phenomena

were mainly accumulated in central areas except for Shanxi and Henan provinces (Figure 5). The population hollowing was slight around the boundaries of the study areas because those regions are close to an urban agglomeration with well economic development that supplies plenty of job opportunities for residents. So, few people living in the marginal areas of the study area would like to immigrate to other cities to make a living. On the contrary, the population hollowing of the inner places was obviously severe for the location and the distance from the urban areas (Figure 6) [81,82].

Secondly, the topography and physical geographic conditions generated significant impacts on human activities. For example, the results obtained by us showed that the population hollowing was serious in the Fenwei Plain, followed by Lvliang Mountains and Taihang Mountains located in Shanxi Province. The possible reasons for the severe population hollowing are stated as follows. The large population and inadequate economic development of Fenwei Plain led to the loss of residents. Meanwhile, the undeveloped infrastructure facilities of the Lv Liang and Taihang Mountains severely limited the local economic development, which resulted in a large number of people living in mountain areas immigrating to urban areas to find jobs. Moreover, although the rank of GDP and the agricultural products of Henan Province is higher than a majority of provinces of China, a dense population leads to the limited capability of resources sustaining [83]. Hence, the population hollowing of Henan province was severe, which was consistent with the conclusion of the current study (Figure 5). Fortunately, the population hollowing of Henan province is decreasing during the past five years according to the trend analysis in Section 3.4 due to continued economic development and well physical geographic conditions.

Last but not least, the population of immigrants is not only influenced by natural and human factors but also affected by national strategies for regional revitalization, national measures for eliminating poverty, and emergencies or disasters [84]. The outcomes of our study indicated the population hollowing of the entire study area is decreasing year by year (Figure 7). Especially, the population hollowing of the six provinces has been significantly reduced from 2019 to 2020. The Chinese government has released a strategy named Plan for Promoting the Rise of central China (2016–2025) to solve the imbalance in the regional development of China. Furthermore, the Targeted Poverty Alleviation Plan of China was published in 2013, and the central government of Chinese has disclosed that the plan was to be finished in the year 2020. Unexpectedly, the COVID-19 pandemic exhibited seriously negative effects on the economy and humans globally. A large number of people had to move to a safe area to protect themselves, and plenty of the population went home during the epidemic period [85]. Consequently, the population hollowing revealed a significant decreasing trend in the study area due to the above-mentioned reasons.

5.3. Limitations of the Current Study

Though several findings have been obtained by the current study, some uncertainties need to be solved further. First, six indicators for PHI at the township scale and twenty dependent variables for PHI at the grid scale were used for determining the population hollowing in the present study. Nevertheless, population hollowing is a complicated issue that may be influenced by both natural and human factors [86]. So, the comprehensive definition of PHI needs to be further developed for well understanding the PHI. Second, the limitations of data used in the current study may result in biases in the study results. The possible reasons for outliers in Figure 4i–h are as follows. The transit time of nighttime light remotely sensed satellite is about 1 a.m. local time, and the majority of lights for illumination have been turned off because the residents always rest after 22 o'clock. So, the PHI value may be overestimated when we used nighttime light remotely sensed images to infer human activities. Additionally, the resolution of some dependent variables was inadequate for describing the PHI. For example, the meteorological and pollution data used in this study were obtained via the kriging interpolation method, which may limit the accuracy of the calibrated models [87]. Third, the identification of potential population hollowing areas may have uncertainties. For example, the PHI of the industrial zone may be

overestimated because the brightness and density of the lights are not very high. Contrarily, the PHI of tourism sites and airports may be underestimated because the lights are always bright, but the population density is low [88].

Overall, the mechanism of population hollowing is complicated, and detailed studies need to be conducted in the future [89]. Hence, the PHI will be strengthened for comprehensively understanding the meaning of the population hollowing phenomenon. Moreover, the high-resolution dataset of the potential variables will be used to promote the accuracy of estimation methods [90]. For example, detailed information concerning sectoral GDP, including industrial GDP, commercial GDP, and services GDP, can be adopted to address the low accuracy of nighttime light images in estimating economic activities in the daytime. Furthermore, the accuracy of population hollowing area determination will be improved in the future via detailed analysis.

6. Conclusions

The present study identified the population hollowing using POI data, nighttime light remotely sensed images, statistical data, and auxiliary data based on multiple models across six provinces in central China during 2016–2020. Some conclusions were obtained. Firstly, the PHI was determined based on the entropy method, and the results showed that the potential population hollowing regions were mainly distributed in rural areas of the study area. Secondly, the simulation accuracy of random forest in estimating PHI outperformed the geographically weighted regression model and multiple linear regression model. Thirdly, the spatial distribution of population hollowing at township scale and grid-scale is basically consistent. The spatiotemporal distribution of population hollowing in central China presented significant characteristics that the PHI value was high in the north and low in the south of the study area, and the PHI value was decreased in the north and increased in the south from 2016 to 2020. The population hollowing value of Shanxi Province and Henan Province was the highest and exhibited the most severe level. Moreover, the remaining four provinces, including Anhui, Hubei, Hunan, and Jiangxi province, also indicated severe population hollowing conditions in central parts. Fourthly, the dynamic of PHI of Henan Province demonstrated the fastest reduction trend during the past five years. On the contrary, the speedy increase in PHI was identified in the southwest of Hubei Province and the north of Jiangxi Province. Overall, the PHI value reduced significantly across the entire study area from 2019 to 2020. The findings of this study urge local governments to pay more attention to the population hollowing issue. Meanwhile, the scheme used in the current study supplies an economical and efficient method to simulate and detect the distribution and dynamics of population hollowing using spatiotemporal datasets. Meanwhile, the outcomes of this work can support governments in making decisions for realizing the strategy of rural vitalization.

Author Contributions: B.G.: Methodology, Writing—original draft, Writing—review and editing, Conceptualization, Supervision. Y.B.: Investigation, Data curation, Visualization, Software, Writing—original draft. L.P.: Investigation, Writing—review and editing. X.Z.: Writing—review and editing. D.Z.: Data curation, Visualization. W.Z.: Validation. X.G.: Data Curation. Q.C.: Supervision, Resources, Founding Acquisition. All authors have read and agreed to the published version of the manuscript.

Funding: This work was supported by the Fundamental Research Funds for the Central Universities, CHD, and Foundation of Shaanxi Key Laboratory of Land Consolidation of Chang'an University (300102352505), Soft Science Research Program of Shaanxi Province, (2022KRM034), and the Natural Science Foundation of Shaanxi Province (2021JM-388).

Institutional Review Board Statement: Not applicable.

Informed Consent Statement: All the participants were given an informed consent to be signed upon they consented to participate in this study.

Data Availability Statement: The data presented in this study are available on request from the corresponding author. The data are not publicly available due to privacy considerations.

Acknowledgments: We appreciate Tingting Xie and Shixin Zhang for editing the manuscript. We also thank all editors and reviewers' constructive suggestions.

Conflicts of Interest: The authors declare that they have no known competing financial interest or personal relationships that could have appeared to influence the work reported in this paper.

References

- Hu, L. Research on Optimal Strategy of Agricultural Products Marketing. *J. Innov. Soc. Sci. Res.* **2021**, *8*, 29–33. [\[CrossRef\]](#)
- Tan, X. Thinking and Practice of Village Tourism Development Planning under the Strategy of Rural Revitalization—A Case Study of Rural Tourism Development Planning in Dongqiao Village, Wuxi County, Chongqing. *Sustain. Dev.* **2020**, *10*, 182–186. [\[CrossRef\]](#)
- Ying, L.; Shu, L.; Li, P. The Hollowing Process of Rural Communities in China: Considering the Regional Characteristic. *Land* **2021**, *10*, 911.
- Liu, Y.; Liu, Y. Geographical research and optimizing practice of rural hollowing in China. *Acta Geogr. Sin.* **2009**, *64*, 1193–1202.
- Liu, Y.; Liu, Y.; Chen, Y.; Long, H. The process and driving forces of rural hollowing in China under rapid urbanization. *J. Geogr. Sci.* **2010**, *20*, 876–888. [\[CrossRef\]](#)
- Liu, Y.; Liu, Y. Progress and Prospect on the Study of Rural Hollowing in China. *Geogr. Res.* **2010**, *29*, 35–42.
- Zhang, W.; Lu, Z.; Yuan, X.; Wang, C.; Gu, Y.; Xu, H.; Streets, D.G. Black carbon emissions from biomass and coal in rural China. *Atmos. Environ.* **2018**, *176*, 158–170. [\[CrossRef\]](#)
- Long, H. Land consolidation: An indispensable way of spatial restructuring in rural China. *J. Geogr. Sci.* **2014**, *24*, 211–225. [\[CrossRef\]](#)
- Tang, C.; Hua, H.; Zhou, G.; Zeng, S.; Xiao, L. The research on optimization mode of spatial organization of rural settlements oriented by life quality. *Acta Geogr. Sin.* **2014**, *69*, 1459–1472.
- Feng, Y.; Ma, J. Rural Ecological Landscape Construction from the Perspective of Rural Revitalization Strategy. *J. Landsc. Res.* **2018**, *10*, 135–137.
- Liu, Y. Research on the urban-rural integration and rural revitalization in the new era in China. *Acta Geogr. Sin.* **2018**, *73*, 637–650.
- Zhang, T.; Wang, Y.; Liu, Y.; Zhao, M. Establishing an economic insurance system under a multiple dynamic evolution mechanism after rural hollowing renovation. *Resour. Sci.* **2016**, *38*, 799–813.
- Guo, B.; Bian, Y.; Zhang, D.; Su, Y.; Wang, X.; Zhang, B.; Wang, Y.; Chen, Q.; Wu, Y.; Luo, P. Estimating Socio-Economic Parameters via Machine Learning Methods Using Luojia1-01 Nighttime Light Remotely Sensed Images at Multiple Scales of China in 2018. *IEEE Access* **2021**, *9*, 34352–34365. [\[CrossRef\]](#)
- Liang, H.; Guo, Z.; Wu, J.; Chen, Z. GDP spatialization in Ningbo City based on NPP/VIIRS night-time light and auxiliary data using random forest regression. *Adv. Space Res.* **2020**, *65*, 481–493. [\[CrossRef\]](#)
- Zhu, X.; Li, Q.; Shen, M.; Chen, J.; Wu, J. A methodology for multiple cropping index extraction based on NDVI time-series. *Nat. Resour.* **2008**, *23*, 534–544.
- Guo, B.; Zhang, D.; Zhang, D.; Su, Y.; Wang, X.; Bian, Y. Detecting spatiotemporal dynamic of regional electric consumption using NPP-VIIRS nighttime stable light data—A case study of Xi'an, China. *IEEE Access* **2020**, *8*, 171694–171702. [\[CrossRef\]](#)
- Wang, C.; Chen, Z.; Yang, C.; Li, Q.; Wu, Q.; Wu, J.; Zhang, G.; Yu, B. Analyzing parcel-level relationships between Luojia 1-01 nighttime light intensity and artificial surface features across Shanghai, China: A comparison with NPP-VIIRS data. *Int. J. Appl. Earth Obs. Geoinf.* **2020**, *85*, 101989. [\[CrossRef\]](#)
- Niu, T.; Chen, Y.; Yuan, Y. Measuring urban poverty using multi-source data and a random forest algorithm: A case study in Guangzhou. *Sustain. Cities Soc.* **2020**, *54*, 102014. [\[CrossRef\]](#)
- Zhang, F.; Zhang, D.; Liu, Y.; Lin, H. Representing place locales using scene elements. *Computers. Environ. Urban Syst.* **2018**, *71*, 153–164. [\[CrossRef\]](#)
- Joshua, B.; Gabriel, C.; Robert, O. Predicting poverty and wealth from mobile phone metadata. *Science* **2015**, *350*, 1073–1076.
- Long, Y.; Shen, Z. *Geospatial Analysis to Support Urban Planning in Beijing*; Springer: Cham, Switzerland, 2015; Volume 116, pp. 1–272.
- Hu, L.; He, S.; Han, Z.; Xiao, H.; Su, S.; Weng, M.; Cai, Z. Monitoring housing rental prices based on social media: An integrated approach of machine-learning algorithms and hedonic modeling to inform equitable housing policies. *Land Use Policy* **2019**, *82*, 657–673. [\[CrossRef\]](#)
- Ye, T.; Zhao, N.; Yang, X.; Ouyang, Z.; Liu, X.; Chen, Q.; Hu, K.; Yue, W.; Qi, J.; Li, Z.; et al. Improved population mapping for China using remotely sensed and points-of-interest data within a random forests model. *Sci. Total Environ.* **2019**, *658*, 936–946. [\[CrossRef\]](#) [\[PubMed\]](#)
- Levin, N.; Duke, Y. High spatial resolution night-time light images for demographic and socio-economic studies. *Remote Sens. Environ.* **2012**, *119*, 1–10. [\[CrossRef\]](#)
- Yu, B.L.; Lian, T.; Huang, Y.X.; Yao, S.J.; Ye, X.Y.; Chen, Z.Q.; Yang, C.S.; Wu, J.P. Integration of nighttime light remote sensing images and taxi GPS tracking data for population surface enhancement. *Int. J. Geogr. Inf. Sci.* **2019**, *33*, 687–706. [\[CrossRef\]](#)

26. Zhang, Y.; Li, Y.; Chen, Y.; Liu, S.; Yang, Q. Spatiotemporal Heterogeneity of Urban Land Expansion and Urban Population Growth under New Urbanization: A Case Study of Chongqing. *Int. J. Environ. Res. Public Health* **2022**, *19*, 7792. [\[CrossRef\]](#) [\[PubMed\]](#)
27. Liu, J.; Zhang, X.; Lin, J.; Li, Y. Beyond government-led or community-based: Exploring the governance structure and operating models for reconstructing China's hollowed villages. *J. Rural Stud.* **2022**, *93*, 273–286. [\[CrossRef\]](#)
28. Hu, T.; Wang, T.; Yan, Q.Y.; Chen, T.X.; Jin, S.G.; Hu, J. Modeling the spatiotemporal dynamics of global electric power consumption (1992–2019) by utilizing consistent nighttime light data from DMSP-OLS and NPP-VIIRS. *Appl. Energy* **2022**, *322*, 119473. [\[CrossRef\]](#)
29. Lu, L.; Weng, Q.; Xie, Y.; Guo, H.; Li, Q. An assessment of global electric power consumption using the Defense Meteorological Satellite Program-Operational Linescan System nighttime light imagery. *Energy* **2019**, *189*, 116351. [\[CrossRef\]](#)
30. Jiang, L.G.; Liu, Y.; Wu, S.; Yang, C. Study on Urban Spatial Pattern Based on DMSP/OLS and NPP/VIIRS in Democratic People's Republic of Korea. *Remote Sens.* **2021**, *13*, 4879. [\[CrossRef\]](#)
31. Mills, G.; Pleijel, H.; Malley, C.S.; Sinha, B.; Cooper, O.R.; Schultz, M.G.; Neufeld, H.S.; Simpson, D.; Sharps, K.; Feng, Z.; et al. Tropospheric Ozone Assessment Report: Present-day tropospheric ozone distribution and trends relevant to vegetation. *Elem. Sci. Anth.* **2018**, *6*, 47. [\[CrossRef\]](#)
32. Zhao, N.; Liu, Y.; Cao, G.; Samson, E.L.; Zhang, J. Forecasting China's GDP at the pixel level using nighttime lights time series and population images. *GIScience Remote Sens.* **2017**, *54*, 407–425. [\[CrossRef\]](#)
33. Shi, K.; Chang, Z.; Chen, Z.; Wu, J.; Yu, B. Identifying and evaluating poverty using multisource remote sensing and point of interest (POI) data: A case study of Chongqing, China. *J. Clean. Prod.* **2020**, *255*, 120245. [\[CrossRef\]](#)
34. Ingacheva, A.; Kokhan, V. Mapping China's ghost cities through the combination of nighttime satellite data and daytime satellite data. In Proceedings of the 32nd European Conference on Modelling and Simulation (ECMS), Wilhelmshaven, Germany, 22–25 May 2018.
35. Cheng, L.; Feng, W.Y.; Jiang, L.H. The Analysis of Rural Settlement Hollowizing System of the Southeast of Taiyuan Basin. *Acta Geogr. Sin.* **2001**, *56*, 437–446.
36. Long, H.; Li, Y.R.; Liu, Y.S. Analysis of Evolutive Characteristics and Their Driving Mechanism of Hollowing Villages in China. *Acta Geogr. Sin.* **2009**, *64*, 1203–1213.
37. Jie, Y.W.; Yan, S.L.; Yang, F.C. Empirical analysis on influencing factors of the hollowing village degree: Based on the survey data of sample villages in Shandong province. *J. Nat. Resour.* **2013**, *28*, 10–18.
38. Song, W.; Chen, B.M.; Zhang, Y. Typical survey and analysis on influencing factors of village-hollowing of rural housing land in China. *Geogr. Res.* **2013**, *32*, 20–28.
39. Yu, Z.; Xiao, L.; Chen, X.; He, Z.; Guo, Q.; Vejre, H. Spatial restructuring and land consolidation of urban-rural settlement in mountainous areas based on ecological niche perspective. *J. Geogr. Sci.* **2018**, *28*, 131–151. [\[CrossRef\]](#)
40. Chung, S.H. Population Change and Risk of Regional Extinction in Gangwon Province. *J. Soc. Sci.* **2019**, *58*, 3–22. [\[CrossRef\]](#)
41. Liu, S.; Bai, M.; Yao, M.; Huang, K. Identifying the natural and anthropogenic factors influencing the spatial disparity of population hollowing in traditional villages within a prefecture-level city. *PLoS ONE* **2021**, *16*, 4. [\[CrossRef\]](#)
42. Lee, J.; Suh, K. A New Index to Assess Vulnerability to Regional Shrinkage (Hollowing out) Due to the Changing Age Structure and Population Density. *Sustainability* **2021**, *13*, 9382. [\[CrossRef\]](#)
43. Tan, X.; Yu, S.Y.; Ouyang, Q.L.; Mao, K.B.; He, Y.H.; Zhou, G.H. Assessment and influencing factors of rural hollowing in the rapid urbanization region: A case study of Chang sha-Zhuzhou-Xiangtan urban agglomeration. *Geogr. Res.* **2017**, *36*, 684–694.
44. Leng, B.-B.; Le, X.-L.; Yuan, G.; Ji, X.-Q. The economic support index evaluation study on the pig breeding scale of the six provinces in central China. *IOP Conf. Ser. Earth Environ. Sci.* **2017**, *94*, 12053. [\[CrossRef\]](#)
45. Wang, Z.; Zhang, F.; Wu, F. Intergroup neighbouring in urban China: Implications for the social integration of migrants. *Urban Stud.* **2016**, *53*, 651–668. [\[CrossRef\]](#)
46. Leng, B.; Ji, X.; Huang, L. Evaluation research on natural resource supply index of the pig breeding scale in the six provinces of central China. *IOP Conf. Ser. Earth Environ. Sci.* **2017**, *81*, 12106. [\[CrossRef\]](#)
47. Qiu, L.; Xiao, H. Notice of retraction a feasibility study on the service economy in the rise of central China. In Proceedings of the 2009 International Conference on Management and Service Science, Wuhan/Beijing, China, 20–22 September 2009.
48. Chen, Z.; Yu, B.; Yang, C.; Zhou, Y.; Yao, S.; Qian, X.; Wang, C.; Wu, B.; Wu, J. An Extended TimeSeries (2000–2018) of Global NPP-VIIRS-like Nighttime Light Data from a Cross-Sensor Calibration. *Earth Syst. Sci. Data* **2021**, *13*, 889–906. [\[CrossRef\]](#)
49. Liu, H.; Liu, X. Establishment of a New Spatial Agglomeration of an Open Economy: Theoretical Basis, Historical Practice and Feasible Pathways. *Contemp. Soc. Sci.* **2020**, *4*, P1–P24.
50. Guo, B.; Zhang, D.; Pei, L.; Su, Y.; Wang, X.; Bian, Y.; Zhang, D.; Yao, W.; Zhou, Z.; Guo, L. Estimating PM_{2.5} Concentrations via Random Forest Method Using Satellite, Auxiliary, and Ground-level Station Dataset at Multiple Temporal Scales across China in 2017. *Sci. Total Environ.* **2021**, *778*, 146288. [\[CrossRef\]](#)
51. Zhang, G.; Guo, X.; Li, D.; Jiang, B. Evaluating the Potential of LJ1-01 Nighttime Light Data for Modeling Socio-Economic Parameters. *Sensors* **2019**, *19*, 1465. [\[CrossRef\]](#)
52. Wang, Y.; Guo, B.; Pei, L.; Guo, H.J.; Zhang, D.M.; Ma, X.Y.; Yu, Y.; Wu, H.J. The influence of socioeconomic and environmental determinants on acute myocardial infarction (AMI) mortality from the spatial epidemiological perspective. *Environ. Sci. Pollut. Res.* **2022**, 1–18. [\[CrossRef\]](#)

53. Guo, B.; Wang, X.; Zhang, D.; Pei, L.; Zhang, D.; Wang, X. A land use regression application into simulating spatial distribution characteristics of particulate matter (PM_{2.5}) concentration in city of Xi'an, China. *Pol. J. Environ. Stud.* **2020**, *29*, 4065–4076. [\[CrossRef\]](#)
54. Sun, X. Green city and regional environmental economic evaluation based on entropy method and GIS. *Environ. Technol. Innov.* **2021**, *23*, 101667. [\[CrossRef\]](#)
55. Xue, J.; Shi, L.; Wang, H.; Ji, Z.; Shang, H.; Xu, F.; Zhao, C.; Huang, H.; Luo, A. Water abundance evaluation of a burnt rock aquifer using the AHP and entropy weight method: A case study in the Yongxin coal mine, China. *Environ. Earth Sci.* **2021**, *80*, 417. [\[CrossRef\]](#)
56. Hu, Y.; Wu, X. Research on Spatial Differentiation and Influencing Factors of Hollowing Rural Population in Anhui Province. *J. Yunnan Agric. Univ. (Soc. Sci.)* **2020**, *14*, 25–31. (In Chinese)
57. Yin, D.; Gui, J.; Xiangzheng, D.; Feng, W. Multidimensional measurement of poverty and its spatio-temporal dynamics in China from the perspective of development geography. *J. Geogr. Sci.* **2021**, *31*, 130–148.
58. Guo, B.; Wang, Y.; Pei, L.; Yu, Y.; Liu, F.; Zhang, D.; Wang, X.; Su, Y.; Zhang, D.; Zhang, B.; et al. Determining the effects of socioeconomic and environmental determinants on chronic obstructive pulmonary disease (COPD) mortality using geographically and temporally weighted regression model across Xi'an during 2014–2016. *Sci. Total Environ.* **2021**, *756*, 143869. [\[CrossRef\]](#) [\[PubMed\]](#)
59. Song, W.; Jia, H.; Huang, J.; Zhang, Y. A satellite-based geographically weighted regression model for regional PM_{2.5} estimation over the Pearl River Delta region in China. *Remote Sens. Environ.* **2014**, *154*, 1–7. [\[CrossRef\]](#)
60. Pei, L.; Wang, X.; Guo, B.; Guo, H.; Yu, Y. Do air pollutants as well as meteorological factors impact Corona Virus Disease 2019 (COVID-19)? Evidence from China based on the geographical perspective. *Environ. Sci. Pollut. Res.* **2021**, *28*, 35584–35596. [\[CrossRef\]](#)
61. He, Q.; Huang, B. Satellite-based mapping of daily high-resolution ground PM_{2.5} in China via space-time regression modeling. *Remote Sens. Environ.* **2018**, *206*, 72–83. [\[CrossRef\]](#)
62. Steininger, M.; Defries, R.; Belward, A. Satellite estimation of tropical secondary forest above-ground biomass: Data from Brazil and Bolivia. *Int. J. Remote Sens.* **2000**, *21*, 1139–1157. [\[CrossRef\]](#)
63. Zhang, B.; Guo, B.; Zou, B.; Wei, W.; Lei, Y.Z.; Li, T.Q. Retrieving soil heavy metals concentrations based on GaoFen-5 hyperspectral satellite image at an opencast coal mine, Inner Mongolia, China. *Environ. Pollut.* **2022**, *300*, 118981. [\[CrossRef\]](#)
64. Guo, B.; Zhang, B.; Su, Y.; Zhang, D.; Wang, Y.; Bian, Y.; Suo, L.; Guo, X.; Bai, H. Retrieving zinc concentrations in topsoil with reflectance spectroscopy at Opencast Coal Mine sites. *Sci. Rep.* **2021**, *11*, 19909. [\[CrossRef\]](#) [\[PubMed\]](#)
65. Breiman, L. Random Forests. *Mach. Learn.* **2001**, *45*, 5–32.
66. Zheng, D.; Rademacher, J.; Chen, J.; Crow, T.; Bresee, M.; Moine, J.L.; Ryu, S. Estimating aboveground biomass using Landsat 7 ETM+ data across a managed landscape in northern Wisconsin, USA. *Remote Sens. Environ.* **2004**, *93*, 402–411. [\[CrossRef\]](#)
67. Ham, J.; Chen, Y.; Crawford, M.M.; Ghosh, J. Investigation of the random forest framework for classification of hyperspectral data. *IEEE Trans. Geosci. Remote Sens.* **2005**, *43*, 492–501. [\[CrossRef\]](#)
68. Wei, J.; Li, Z.; Cribb, M.; Huang, W.; Xue, W.; Sun, L.; Guo, J.; Peng, Y.; Li, J.; Lyapustin, A.; et al. Improved 1 km resolution PM_{2.5} estimates across China using enhanced space-time extremely randomized trees. *Atmos. Chem. Phys.* **2020**, *20*, 3273–3289. [\[CrossRef\]](#)
69. Xu, Z. Influencing Factors and Urbanization Effects of the Spatial Pattern of Floating Population in Anhui Province. *J. Landsc. Res.* **2019**, *11*, 88–98.
70. Dotto, A.; Dalmolin, R.; Ten Caten, A.; Grunwald, S. A systematic study on the application of scatter-corrective and spectral-derivative preprocessing for multivariate prediction of soil organic carbon by Vis-NIR spectra. *Geoderma* **2018**, *314*, 262–274. [\[CrossRef\]](#)
71. Guo, B.; Wang, X.; Pei, L.; Su, Y.; Zhang, D.; Wang, Y. Identifying the spatiotemporal dynamic of PM_{2.5} concentrations at multiple scales using geographically and temporally weighted regression model across China during 2015–2018. *Sci. Total Environ.* **2021**, *751*, 141765. [\[CrossRef\]](#)
72. Guo, B.; Su, Y.; Pei, L.; Wang, X.; Zhang, B.; Zhang, D.; Wang, X. Ecological risk evaluation and source apportionment of heavy metals in park playgrounds: A case study in Xi'an, Shaanxi Province, a northwest city of China. *Environ. Sci. Pollut. Res.* **2020**, *27*, 24400–24412. [\[CrossRef\]](#)
73. Guo, B.; Su, Y.; Pei, L.; Wang, X.; Wei, X.; Zhang, B.; Zhang, D.; Wang, X. Contamination, Distribution and Health Risk Assessment of Risk Elements in Topsoil for Amusement Parks in Xi'an, China. *Pol. J. Environ. Stud.* **2021**, *30*, 601–617. [\[CrossRef\]](#)
74. Liang, X.; Tang, X.; Luo, Y.; Zhang, M.; Feng, Z. Effects of policies and containment measures on control of COVID-19 epidemic in Chongqing. *World J. Clin. Cases* **2020**, *8*, 2959–2976. [\[CrossRef\]](#) [\[PubMed\]](#)
75. Hong, Y.; Shen, R.; Cheng, H.; Chen, Y.; Zhang, Y.; Liu, Y.; Zhou, M.; Yu, L.; Liu, Y.; Liu, Y. Estimating lead and zinc concentrations in peri-urban agricultural soils through reflectance spectroscopy: Effects of fractional-order derivative and random forest. *Sci. Total Environ.* **2019**, *651*, 1969–1982. [\[CrossRef\]](#)
76. Wei, J.; Huang, W.; Li, Z.; Xue, W.; Peng, Y.; Sun, L.; Cribb, M. Estimating 1-km resolution PM_{2.5} concentrations across China using the space-time random forest approach. *Remote Sens. Environ.* **2019**, *231*, 111221. [\[CrossRef\]](#)
77. Lan, Z.; Chun, Y. Beautiful Village Planning and Construction: A Practice of Human Settlement Improvement in Jiangsu Province. *China City Plan. Rev.* **2014**, *23*, 40–50.

78. Peng, J.; Chen, S.; Lü, H.; Liu, Y.; Wu, J. Spatiotemporal patterns of remotelysensed PM_{2.5} concentrations in China from 1999 to 2011. *Remote Sens. Environ.* **2016**, *174*, 109–121. [[CrossRef](#)]
79. Xie, H.; Zou, J.; Peng, X. Spatial-temporal difference analysis of cultivated land use intensity based on emergy in Poyang Lake eco-economic zone. *ActaGeograph. Sin.* **2012**, *67*, 889–902.
80. Rodríguez-Puerta, F.; Alonso Ponce, R.; Pérez-Rodríguez, F.; Águeda, B.; Martín-García, S.; Martínez-Rodrigo, R.; Lizarralde, I. Comparison of Machine Learning Algorithms for Wildland-Urban Interface Fuelbreak Planning Integrating ALS and UAV-Borne LiDAR Data and Multispectral Images. *Drones* **2020**, *4*, 21. [[CrossRef](#)]
81. Ganggayah, M.; Taib, N.; Har, Y.; Lio, P.; Dhillon, S. Predicting factors for survival of breast cancer patients using machine learning techniques. *BioMed. Cent.* **2019**, *19*, 48. [[CrossRef](#)]
82. Qi, W.; Yi, J. Spatial pattern and driving factors of migrants on the Qinghai-Tibet Plateau: Insights from short-distance and long-distance population migrants. *J. Geogr. Sci.* **2021**, *31*, 215–230. [[CrossRef](#)]
83. En, W.; Xue, B.; Yang, J.; Lu, C. Effects of the Northeast China Revitalization Strategy on Regional Economic Growth and Social Development. *Chin. Geogr. Sci.* **2020**, *30*, 791–809.
84. Wu, Q.; Chen, J. The Effect and Influence of Tourism Poverty Alleviation of Residents in Poor Areas: A Case Study of Key Tourism Poverty Alleviation Villages in Northern Guangdong. *J. Landsc. Res.* **2021**, *13*, 89–94.
85. Ye, Y.; Wang, C.; Zhang, H.; Yang, J.; Liu, Z.; Wu, K.; Deng, Y. Spatiotemporal analysis of COVID-19 risk in Guangdong Province based on population migration. *J. Geogr. Sci.* **2020**, *30*, 1985–2001. [[CrossRef](#)]
86. Yin, Y.; Zhang, Y. Environmental Pollution Evaluation of Urban Rail Transit Construction Based on Entropy Weight Method. *Nat. Environ. Pollut. Technol.* **2021**, *20*, 819–824. [[CrossRef](#)]
87. Wang, X.; Li, Y.; Li, Y.; Chen, Y.; Lian, J.; Cao, W. Comparison of sampling schemes for spatial prediction of soil organic carbon in Northern China. *Sci. Cold Arid Reg.* **2020**, *12*, 200–216.
88. Xu, P.; Lin, M.; Jin, P. Spatio-temporal Dynamics of Urbanization in China Using DMSP/OLS Nighttime Light Data from 1992–2013. *Chin. Geogr. Sci.* **2021**, *31*, 70–80. [[CrossRef](#)]
89. Zhao, F.; Ding, J.; Zhang, S.; Luan, G.; Song, L.; Peng, Z.; Du, Q.; Xie, Z. Estimating Rural Electric Power Consumption Using NPP-VIIRS Night-Time Light, Toponym and POI Data in Ethnic Minority Areas of China. *Remote Sens.* **2020**, *12*, 2836. [[CrossRef](#)]
90. Shi, K.; Yu, B.; Huang, C.; Wu, J.; Sun, X. Exploring spatiotemporal patterns of electric power consumption in countries along the Belt and Road. *Energy* **2018**, *150*, 847–859. [[CrossRef](#)]